An annual cycle of Arctic cloud characteristics observed by radar and lidar at SHEBA

J. M. Intrieri,[1] M. D. Shupe,[2] T. Uttal,[1] and B. J. McCarty[3]

[1] The temporal distributions of cloudiness, vertical distribution of cloud boundary heights, and occurrence of liquid phase in clouds are determined from radar and lidar data sets collected from October 1997 to October 1998 during the Surface Heat Budget of the Arctic Ocean (SHEBA) project. The radar/lidar combination was necessary for comprehensive cloud detection over a variety of physical conditions and is significantly more detailed (5–9 s temporal resolution, 30–40 m vertical resolution) than measurements made by surface observers or satellites. The combined measurements revealed that clouds were almost continuously present, with an annual average occurrence of 85%, and displayed an overall annual trend of a cloudier summer and clearer winter. A monthly averaged cloud occurrence maximum of 97% was observed in September and a minimum of 63% was observed in February. Monthly averaged lowest cloud base heights were between 0.25 and 1.0 km above ground level (agl) and monthly averaged highest cloud top heights were between 2.5 and 5.5 km agl, and displayed no significant seasonal variation. The number of cloud layers was typically 1 or 2, with the summer months tending to be multilayered. The lidar utilized depolarization ratios to detect liquid water; the percentage of lidar-observed clouds containing liquid was 73% for the year. The least amount of liquid water phase was observed during December in 25% of the lidar-detected clouds and the maximum was observed during July in 95% of the lidar-detected clouds. Liquid was distributed in a combination of all-liquid and mixed phase clouds, and was detected at altitudes as high as 6.5 km agl and at temperatures as low as $-34°C$. *INDEX TERMS:* 3309 Meteorology and Atmospheric Dynamics: Climatology (1620); 3360 Meteorology and Atmospheric Dynamics: Remote sensing; 1694 Global Change: Instruments and techniques; 3349 Meteorology and Atmospheric Dynamics: Polar meteorology; 3359 Meteorology and Atmospheric Dynamics: Radiative processes; *KEYWORDS:* Lidar, radar, remote sensing, clouds, polar meteorology, climatology

1. Introduction

[2] The Arctic has historically been one of Earth's most scientifically underinvestigated regions, but recently hypothesized links between Arctic ice-atmosphere-ocean processes and global warming have increased research activities in this region. Not only is the Arctic climate thought to have impacts on lower latitude climates, but some large-scale model simulations predict that the Arctic may also be a region where early warning indicators of climate change will be most apparent [*Washington and Meehl*, 1989]. One of the key physical processes under study is the effect Arctic clouds have on the surface heat budget over sea ice [*Curry et al.*, 1996a]. Understanding the effect of clouds on the surface is especially important over the Arctic Ocean because it can significantly impact the melting, refreezing, thickness and distribution of the seasonal ice pack [*Maykut and Unterstiener*, 1971]. Evidence indicates that strong couplings exist between the surface and clouds, however, the magnitudes, and in some cases the sign, of the cloud-radiation feedback mechanisms are still unknown and appear to be a complicated function of cloud height, thickness, phase and particle size [*Francis*, 1999; *Curry and Ebert*, 1992]. Studies have also shown that different cloud parameterizations can cause large discrepancies in simulations of Arctic climate [*Randall et al.*, 1998].

[3] Our understanding of Arctic cloud properties and their impact on radiation fluxes is limited by the fact that little observational data exist on Arctic clouds, especially during the dark winter season. Although satellites can provide the greatest spatial and temporal coverage for characterizing this vast and sparsely observed region, they encounter difficulties in the polar areas due to the poor thermal and visible contrasts between clouds and the underlying snow/ice surface [*Key and Barry*, 1990]. Information from surface observers is sparse in addition to being problematic, particularly during winter when darkness hinders cloud classification [*Hahn et al.*, 1995]. Arctic field programs using aircraft have provided some additional

[1]NOAA/Environmental Technology Laboratory, Boulder, Colorado, USA.
[2]Science and Technology Corporation, NOAA/Environmental Technology Laboratory, Boulder, Colorado, USA.
[3]Cooperative Institute for Research in the Environmental Sciences, University of Colorado, Boulder, Colorado, USA.

information on cloud characteristics [e.g., *Curry et al.*, 1996b; *Hobbs and Rangno*, 1998] however, these data sets are limited in areal and temporal coverage and typically only cover spring and summer months.

[4] In this paper, we present an annual cycle of the vertical and temporal distribution of cloudiness, as well as cloud phase information, that are derived from measurements obtained by two range-resolved active remote sensors: a 523 μm lidar and a 35 GHz millimeter-wave radar. The platform for this yearlong measurement program was a Canadian Coast Guard ship, *Des Groseilliers*, frozen into the Arctic ice pack as part of the Surface Heat Budget of the Arctic Ocean (SHEBA) project [*Perovich et al.*, 1999; *Uttal et al.*, 2002]. In section 2 details of the operational and technical aspects of the radar and lidar are presented. Section 3 describes how the data streams from these two instruments are combined to provide a more comprehensive measurement of the cloud properties than would be possible with either sensor individually. In section 4 the monthly cloud statistics are discussed and conclusions are presented in section 5.

2. Radar and Lidar Technical Details

[5] Both the lidar and radar used during SHEBA were specifically designed for long-term continuous operation under Arctic conditions with an emphasis on the detection of Arctic clouds and a minimum of operator intervention. The lidar is a prototype system, and the radar is nearly identical to the cloud radars which have been designed for the DOE/Atmospheric Radiation Measurement (ARM) program which continuously operates these radars in Alaska, Oklahoma and in the Tropical Western Pacific [*Stokes and Schwartz*, 1994]. Both instruments were designed and built by the NOAA Environmental Technology Laboratory (ETL).

2.1. The Depolarization and Backscatter Unattended Lidar

[6] The lidar system used at SHEBA was the Depolarization and Backscatter Unattended Lidar (DABUL). DABUL is an active remote sensing system that transmits very short pulses of laser light at a green wavelength (523 μm). The energy scattered back to the system yields high resolution information on the horizontal and vertical structure of clouds and aerosols. The combination of low laser-pulse energies and a large beam diameter makes the DABUL system fully eye-safe [*Grund and Sandberg*, 1996; *Alvarez et al.*, 1998]. DABUL was housed in a weatherproof container that was environmentally controlled to protect and stabilize the optics and electronics.

[7] A key feature of the DABUL system is dual polarization states which yield depolarization ratio information that can be used to distinguish between the liquid and solid phases of water in the atmosphere [*Sassen*, 1991]. In general, spherically symmetric particles backscatter energy through a combination of axial reflections and/or surface waves which do not change the incident polarization state. The backscatter from complex shapes is due to internal reflections that rotate the incident polarization state. Thus, small raindrops, water cloud droplets, and fog are spherical and have negligible depolarization signatures. Non-spherical particles such as ice crystals, snowflakes or large oblate raindrops contain a cross-polarized component and can

exhibit depolarization ratios greater than ~20%. An unchanged polarization state between the scattered and incoming radiation can also be a result of scattering from certain crystal shapes and orientations that have reflectional symmetry. For example, oriented ice crystals such as plates can specularly reflect laser light producing small depolarization ratios that might be misinterpreted as a liquid water signature. To compensate for this effect, the lidar was tilted 5 degrees from vertical to prevent ambiguous depolarization signatures.

[8] Cloud base and top heights, for all detected layers, were determined by thresholding the lidar returned power and depolarization ratio fields. After the cloud boundaries were determined, layer-averaged depolarization ratios were calculated for each layer.

[9] Figure 1 shows (a) the 24 hour time-height plot of DABUL depolarization ratios, (2) the layer-averaged depolarization ratios, and (3) the integrated liquid water path from microwave radiometer measurements. Between 0000 and 0800 UTC and 1800 and 2400 UTC the low-level cloud layer at 1 km had lidar depolarization ratios around 0.05 corresponding to times when the microwave radiometer detected liquid water. In the intervening period from 0800 to 1800 UTC the lower cloud layer dissipated and the lidar detected cloud, up to 5 km with depolarization ratios between 0.1 and 0.4, while the radiometer detected no significant liquid in the atmosphere. Based on observations such as these, as well as previous experience with lidar depolarization signatures, we determined that depolarization ratios less than 0.11 indicate liquid water phase and depolarization ratios greater than 0.11 indicate ice phase.

[10] During SHEBA, the lidar was located on the helicopter deck of the *Des Groseilliers*. DABUL operated from 1 November 1997 through 8 August 1998 after which time a laser failure occurred. Two down times of note occurred between 2–12 February (for heater repair) and 5–10 July (for optical shutter disabling), however, data were collected reliably and continuously for the majority of the annual cycle. DABUL collected data between the surface and 20 km above ground level (agl) with a range resolution of 30 m and time averages of 5 s.

2.2. The Millimeter Cloud Radar

[11] The 35 GHz millimeter cloud radar (MMCR) was designed to provide continuous measurement of radar reflectivity, Doppler velocity, and Doppler spectral width. Unlike conventional weather radars with wavelengths on the order of centimeters, this shorter wavelength ($\lambda = 8.66$ mm, K_a-band) is optimized to be sensitive to nonprecipitating clouds and operates in an atmospheric window region. Like DABUL, the MMCR was designed for obtaining long-term, continuous measurements in remote locations with minimum operator interface. The antenna is in a fixed, vertically pointing orientation which is different from many millimeter research radars that typically scan in azimuth and elevation. The MMCR utilizes a low peak-power transmitter with high duty-cycles and a high-gain antenna making it a particularly sensitive system with a detection threshold of −49 dBZ at 5 km range.

[12] The MMCR cycles through four modes which use different combinations of pulse-coding and range resolutions. The high sensitivity modes are optimum for detecting
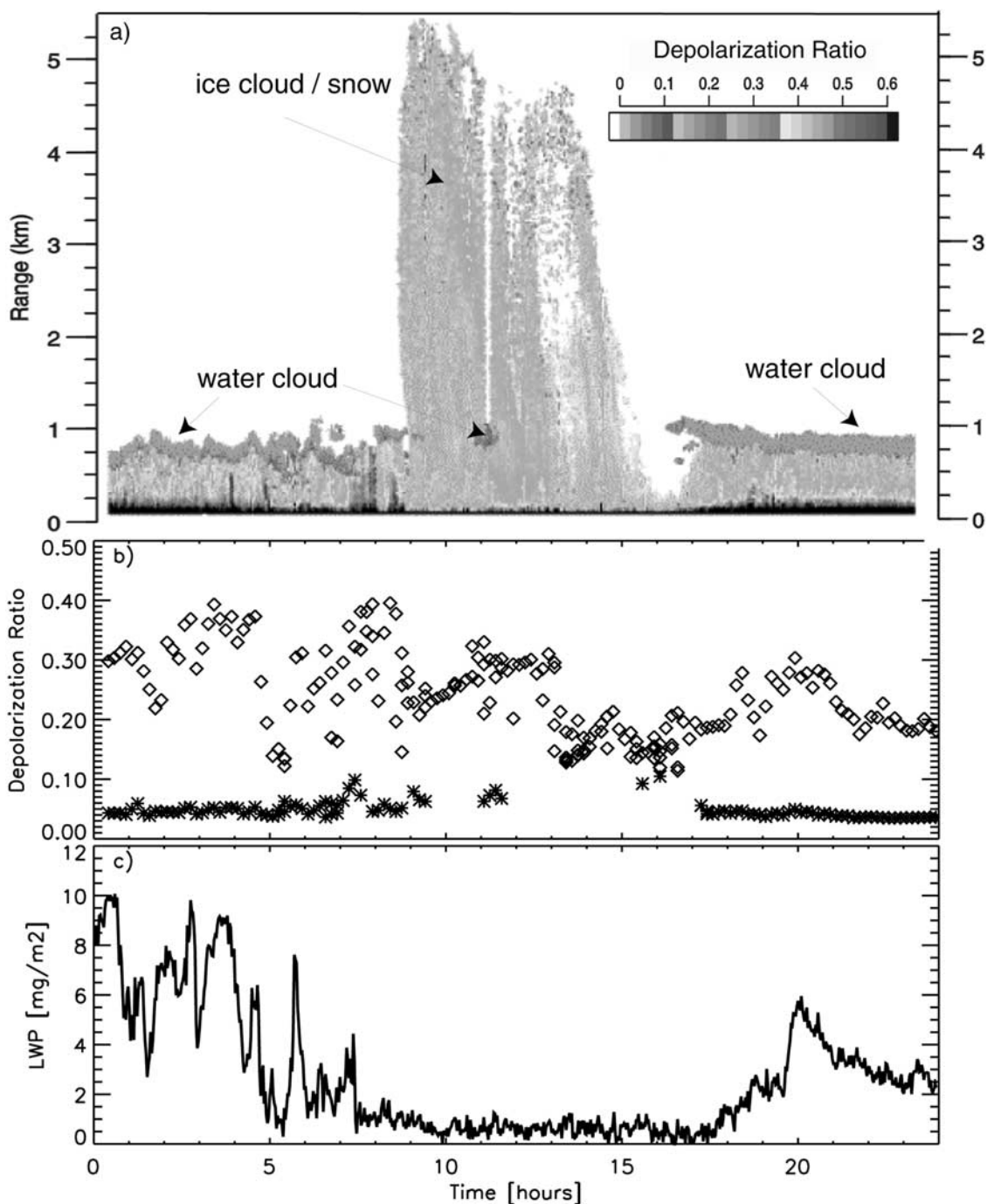
Figure 1. (a) Time-height plot of the lidar depolarization ratio field, (b) corresponding time series of the layer-average depolarization ratio values for the low level water cloud (asterisks) and ice crystal precipitation (diamonds), and (c) time series of microwave radiometer column liquid water amount (mg/ m²) for 6 May 1998. See color version of this figure at back of this issue.

clouds with small particles in low concentrations, but also generate signal artifacts near the ground, near high reflectivity cloud elements, and in regions of strong reflectivity gradient. The low sensitivity modes produce artifact-free measurements of the higher reflectivity clouds, but are not sensitive enough to detect low signal clouds such as high cirrus and ice fogs. The four modes are combined into a single product in postprocessing, using the best mode in each region of the time-height cloud scene. This produces

optimized measurements for a wide range of cloud types. Between the beginning of the project and 8 December 1997, there was a partial failure with the transmission hardware causing losses in the higher sensitivity modes. Reflectivity corrections were applied in postprocessing, however, there were some irretrievable losses of signal from the lowest reflectivity clouds. Therefore, the first two months of radar data may indicate somewhat lower cloud tops than if the unit had been operating optimally.
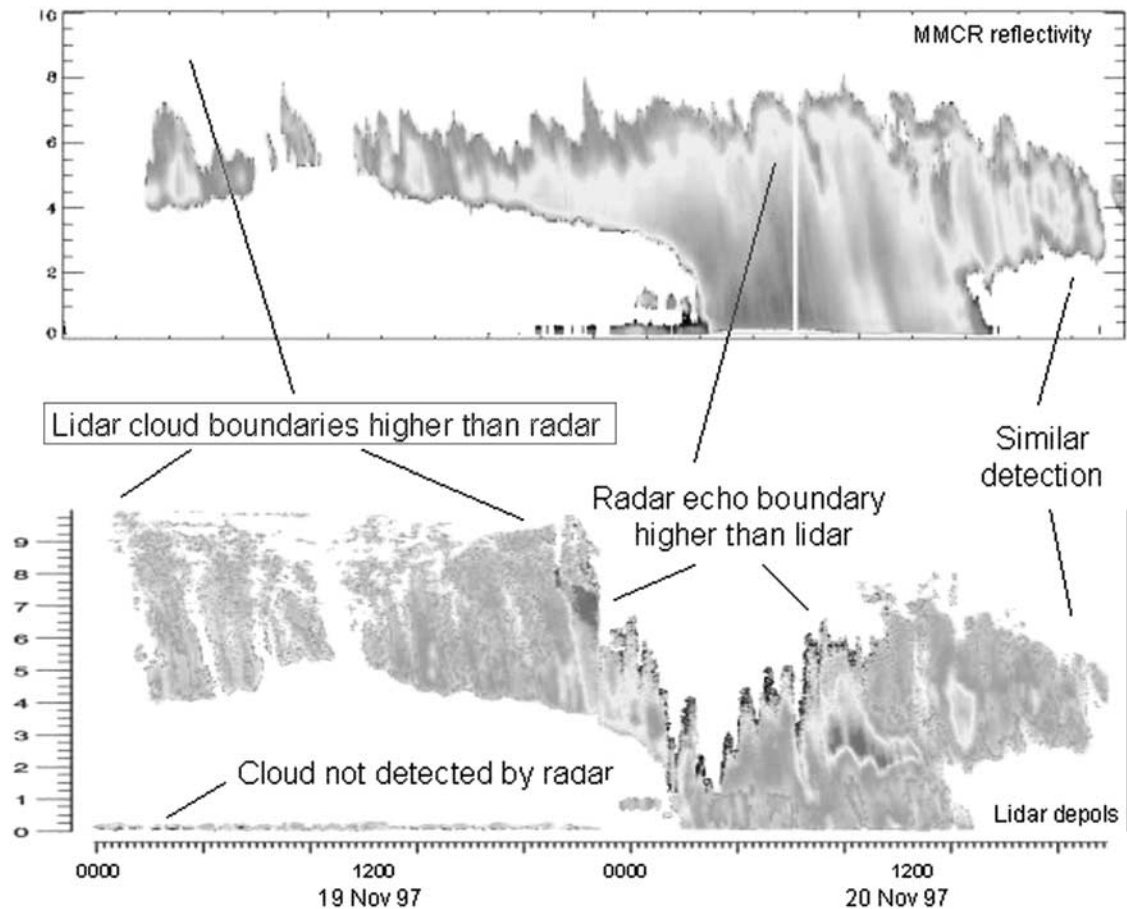
Figure 2. Two day time-height plot of radar reflectivity (top) and lidar depolarization ratio (bottom) for 19–20 November 1997 illustrating the similarities and differences in radar and lidar returns a variety of cloud types. See color version of this figure at back of this issue.

[13] During the SHEBA experiment, the MMCR collected data in 45 m range gates, with 9 s averaging periods, between the surface and 15 km agl. The radar was housed in a seatainer, about 25 feet from the DABUL on the helicopter deck of the *Des Groseilliers*. Technical details concerning the cloud radar are given by *Moran et al.* [1998].

3. Analysis Methods

[14] DABUL and the MMCR have very different detection capabilities which are illustrated in Figure 2 by time-height images of radar reflectivity (upper panel) and lidar depolarization ratio (lower panel) for a 48 hour period in November 1997. During the first 22 hours of the period, the DABUL detected a very thin layer (about 200 m agl) of return at the surface which is only spuriously detected by the radar. This indicates that the layer was composed of an ice fog with particles small enough to be invisible to the radar. During the same period, in the upper level cloud layer, DABUL and MMCR echo bases agree very well, however, DABUL detects a significantly thicker cloud than the MMCR. This difference indicates that the cloud was topped by a region of very small ice crystals that was not detected by the MMCR. At 0200 UTC on 20 November, a 12 hour precipitation event began which attenuated the DABUL signal as much as 5 km lower than the echo tops

detected by the radar. During the final 6 hours of the period, DABUL and the MMCR showed excellent agreement on both cloud base and top heights.

[15] These sometimes substantial differences in echo boundaries detected by the lidar and the radar are a function of the fundamental physical differences between transmitting at optical and millimeter wavelengths. The lidar operates in the Mie scattering regime (particles are large with respect to wavelength) in which signal is sensitive to the cross-sectional or two-dimensional area of the particle. The disadvantage of the system is that it can be severely attenuated due to absorption by large precipitation-sized ice particles and by optically thick liquid cloud layers. The radar operates in the Rayleigh scattering regime (particles are small with respect to the wavelength) in which the signal is sensitive to the 6th power of the particle size. In the Arctic, it was expected that only rare instances of moderate to heavy rain would attenuate the radar, however, even the relatively sensitive MMCR is not able to see very small water droplets or ice crystals in low concentrations that can be detected by the lidar.

[16] Experience indicates that radars often cannot distinguish between precipitation and cloud regions with reflectivity measurements alone, and that lidars have a more accurate measurement of cloud base. On the other hand, because the lidar often is unable to penetrate above layers of optically thick water cloud or heavy snow/ice precipitation,
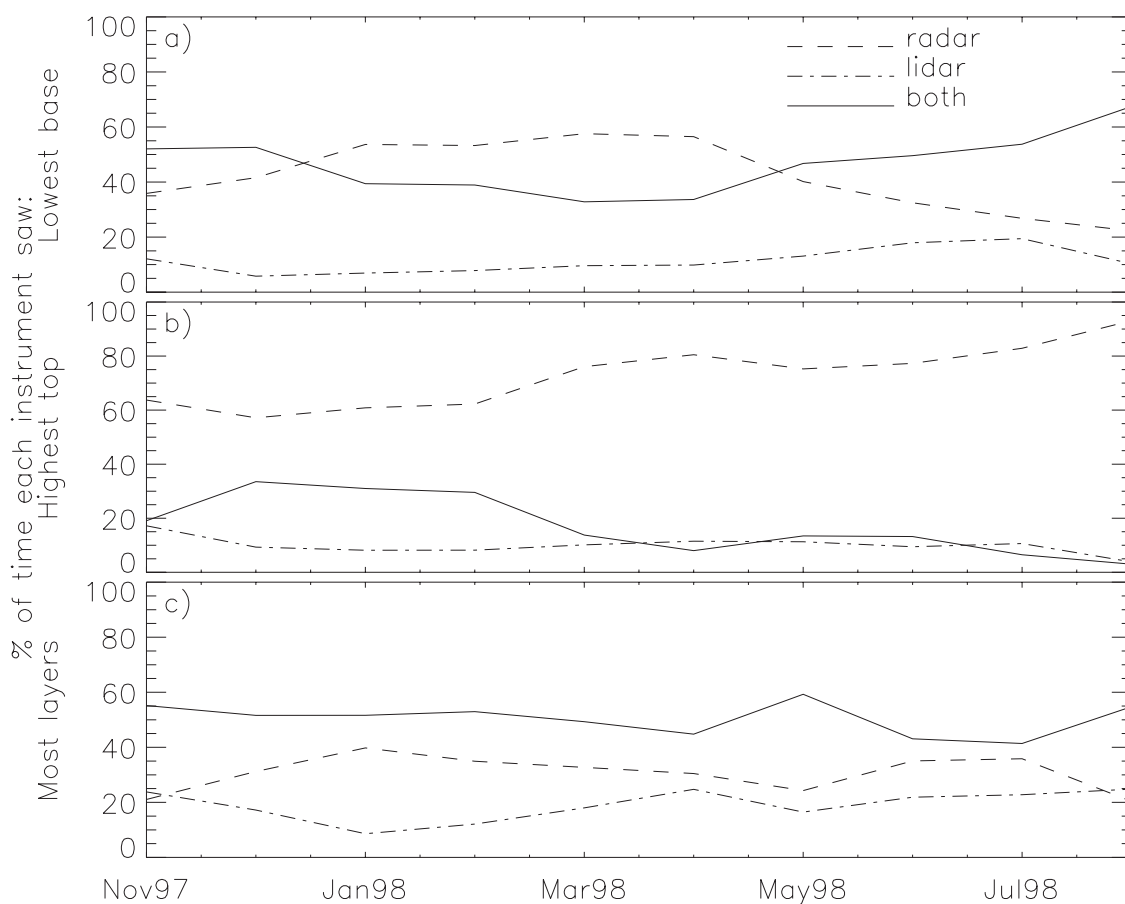
Figure 3. Percentage of time the lidar (dash-dot), radar (dashed line), or both (solid line) instruments detected the (a) lowest cloud base height (km), (b) highest cloud top height (km) and (c) maximum number of cloud layers.

it frequently obtains measurements of cloud top that are biased low, sometimes by several kilometers. Therefore, lidars are better suited to determining the lowest cloud base height and radars are generally the instrument of choice for characterizing the highest cloud top.

[17] In Figure 3, statistics on the relative detection properties of the DABUL and the MMCR are presented for periods during which both instruments were operating. Figure 3a shows that DABUL and the MMCR agreed on the location of cloud base between 30% and 65% of the time which is a rough measure of the percent of time that the clouds were not precipitating. The MMCR saw a lower echo base between 25% and 55% of the time while the lidar detected a lower echo base only about 10–20% of the time. Figure 3b indicates that the MMCR detected the highest echo top between 60% and 95% of the time. The two instruments agreed on the location of echo top height approximately 25% of the time, with the highest percentage of agreement (35%) occurring in winter when there were less liquid cloud layers that attenuated the lidar signal. Finally, DABUL detected tops higher than the MMCR about 15% of the time.

[18] Separate cloud layers were defined as echo regions, with distinct bases and tops, separated by range gates containing no cloud echo for at least 90 m. The DABUL detected more layers approximately 20% of the time and the

MMCR detected more layers around 30% of the time; the two instruments saw the same number of layers about 50% of the time (Figure 3c). Similar work combining radar and lidar measurements to obtain comprehensive cloud boundary values has been reported by *Clothiaux et al.* [2000]. Both this study and the study by *Clothiaux et al.* [2000] demonstrate that it is critical to analytically integrate radar and lidar data sets in order to obtain accurate cloud boundary measurements.

[19] For this paper, statistics on echo base height, top height and number of layers were first determined individually from DABUL (using returned power and depolarization ratio thresholds) and the MMCR (using reflectivity thresholds) to separate cloudy from cloud-free regions of the atmosphere. The lidar and radar data were then combined to produce cloud statistics using following criteria:

1. For lowest cloud base, DABUL base heights were used if DABUL was operating, otherwise, MMCR base heights were used.

2. For highest cloud top, the highest measured echo from either instrument was used.

[20] The largest potential errors occurred for conditions when the radar echo base was used for cloud base height when DABUL was not operating and when DABUL echo top was used for cloud top height when the MMCR was not operating. Figure 4 shows the monthly operating statistics
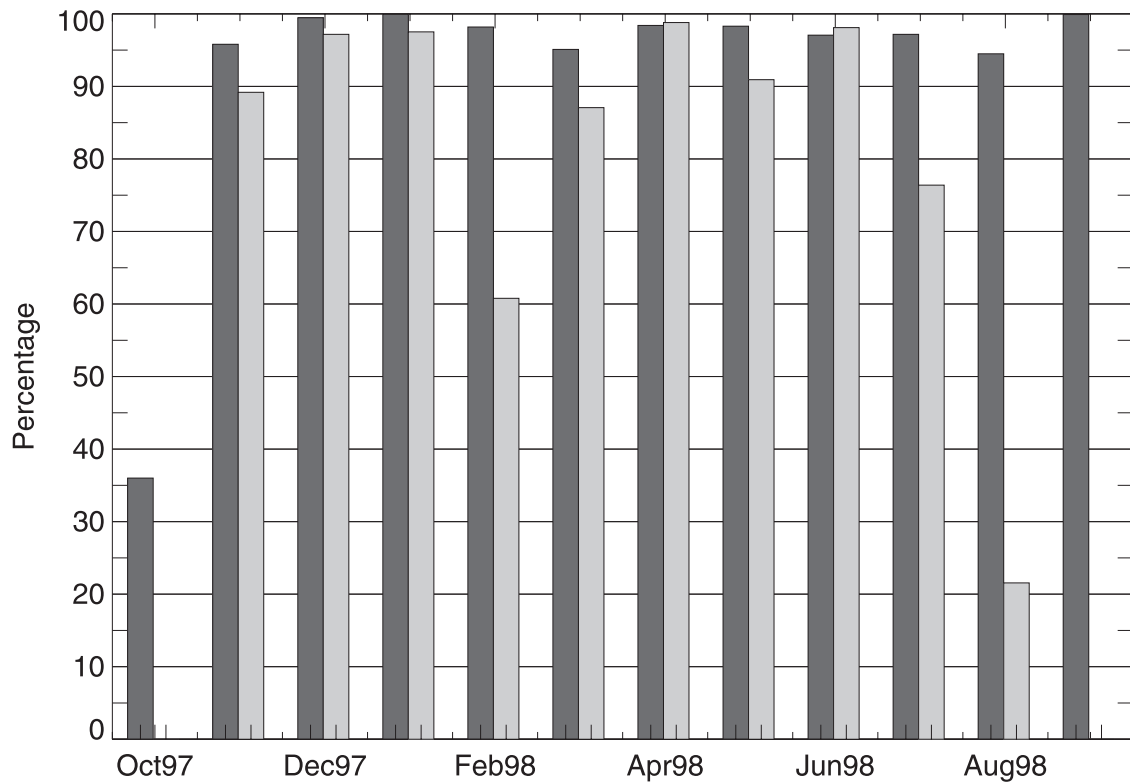
Figure 4. Monthly averaged percentage of time the lidar (light gray bars) and radar (dark gray bars) were operational from October 1997 through September 1998.
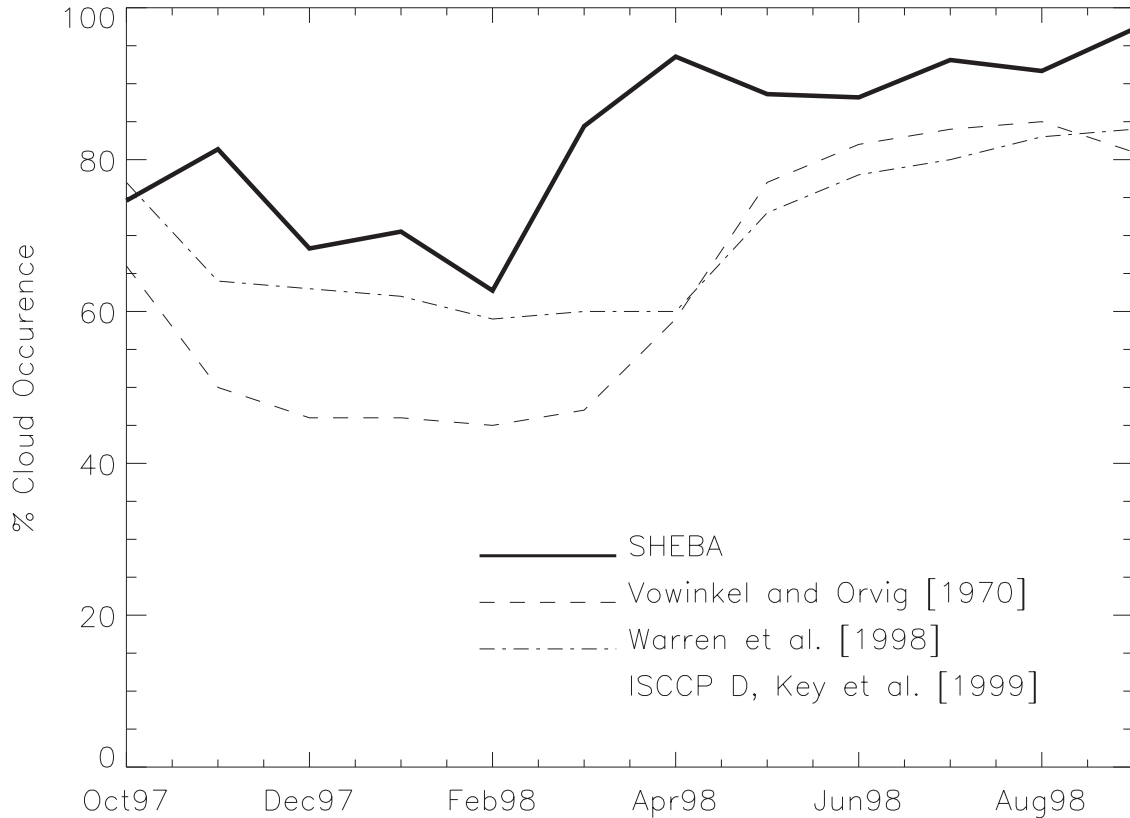

Figure 5. Monthly averaged cloud occurrence percentages from the combined SHEBA lidar-radar data (bold line), surface observations from [*Vowinkel and Orvig*, 1970] (dashed line) and *Warren et al.* [1988] (dash-triple-dot), and satellite data from *Key et al.* [1999] (dash-triple-dot).
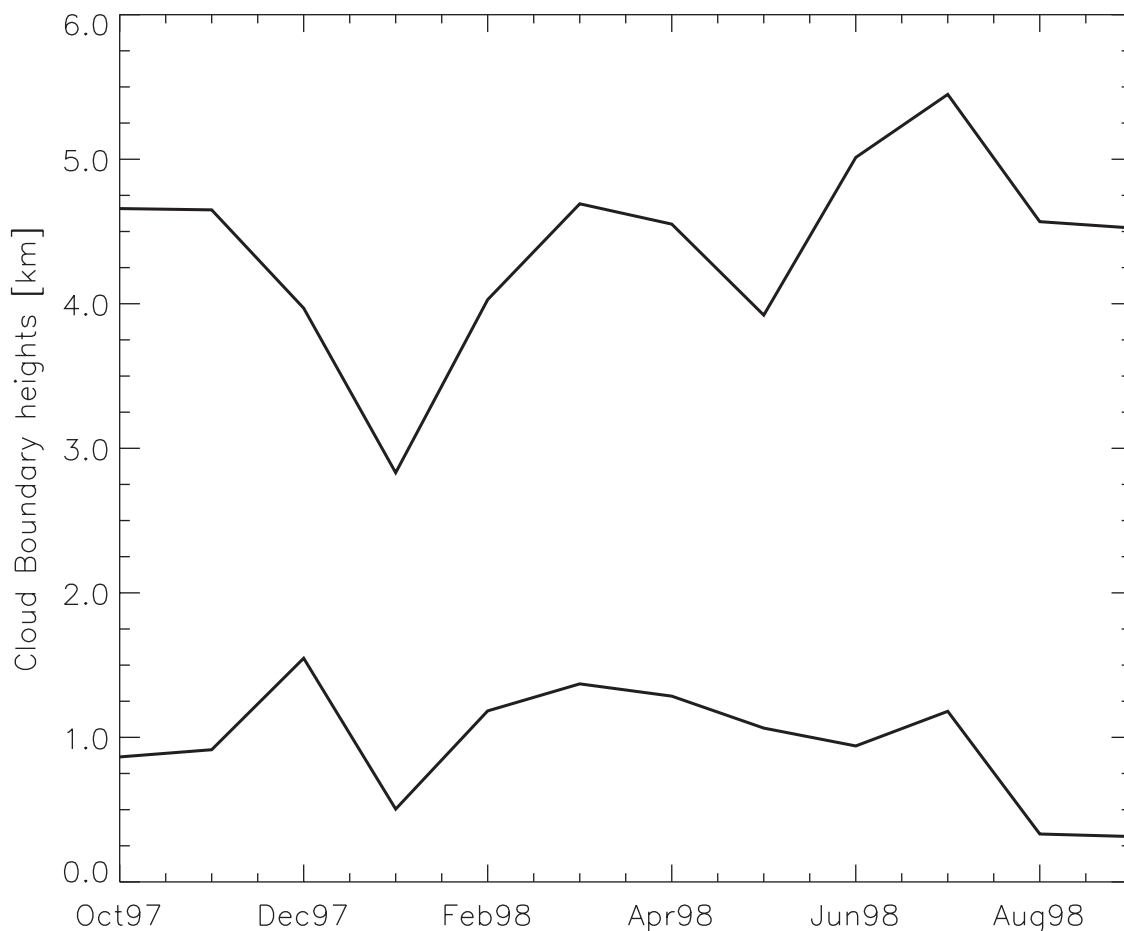
Figure 6.   Monthly averaged cloud base height and cloud top height from the combined lidar-radar data set.

for the two instruments indicating that the MMCR downtimes occurred only occasionally, with DABUL downtimes being more frequent. The effect on monthly statistics presented in the next section is that cloud base height values may be slightly lower by 250–500 m during October, February, August and September. Also, as mentioned in section 2, the monthly statistics on cloud top heights may also be low for October, November and December because of sensitivity problems with the MMCR. Between the two instruments there was essentially 100% data coverage during the SHEBA project, with the MMCR 97% operational over the full measurement period, and the DABUL 82% operational between 1 November 1997 and 8 August 1998. This implies that the monthly statistics on fraction of cloud occurrence (either the MMCR or the DABUL detected return) are quite accurate.

4.   Results

4.1.   Monthly Fraction of Cloud Occurrence

[21]   The monthly fraction of cloud occurrence determined from the combined DABUL and the MMCR data set is shown in Figure 5. Fraction of cloud occurrence is defined as the percentage of time that either the MMCR or DABUL observed cloud over the ice station. It should be noted that this is a fundamentally different value than "cloud fraction", which refers to the percentage of sky that

is covered with clouds at a single instant, as detected by surface observers, hemispheric imagers or in satellite scenes or pixels.

[22]   The monthly fraction of cloud occurrence showed a pronounced annual cycle with late summer and early fall being the cloudiest (maximum of 97% in September) and winter having the least percentage of cloudiness (minimum of 63% in February). The average fraction of cloud occurrence for the entire year was 84%. In interpreting these results it must be kept in mind that the ice station was not stationary, and therefore, the statistics in Figure 5 are a function of both seasonal and regional changes. In particular, during the summer months, the ice station had drifted far to the west, out of the Beaufort Gyre and experienced significant synoptic activity from storms that were passing northward through the Bering Strait.

[23]   Although it is not a direct comparison of the same parameter, existing climatologies of Arctic cloud fractions using satellite data from *Key et al.* [1999] and surface-based climatological observations [*Vowinkel and Orvig*, 1970; *Warren et al.*, 1988], are also plotted in Figure 5. These climatological data sets show generally less cloud cover, ranging from 80% in summer to 40–60% in winter. These values may be lower for a number of reasons including lower detection rates, especially during winter, by surface observers, scene identification problems over the ice/snow surface associated with satellite techniques, as well as
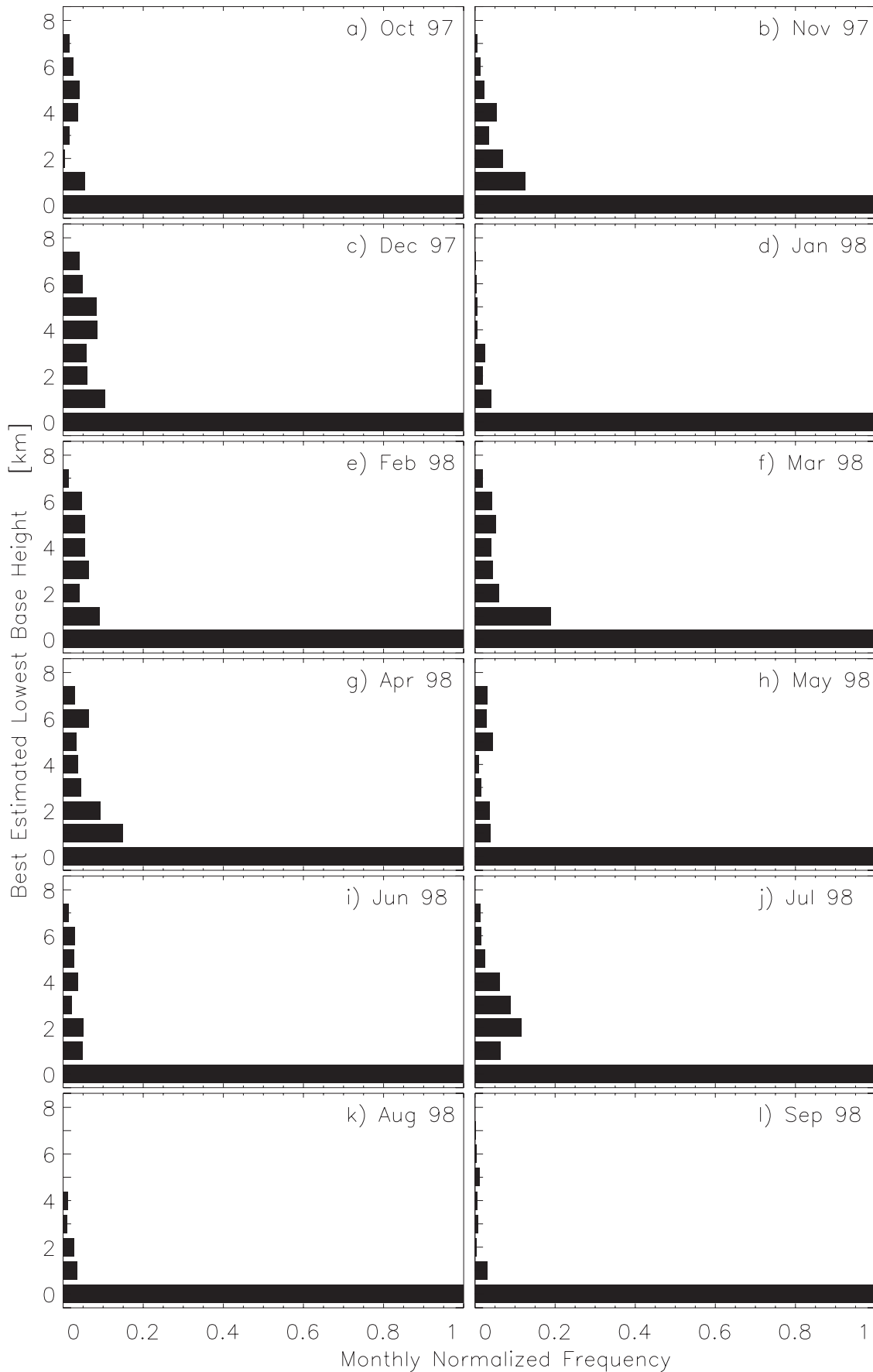
Figure 7. (a–l) Frequency distribution of lowest cloud base height (km) as a function of altitude for October 1997 through September 1998. Bin size = 0.5 km.
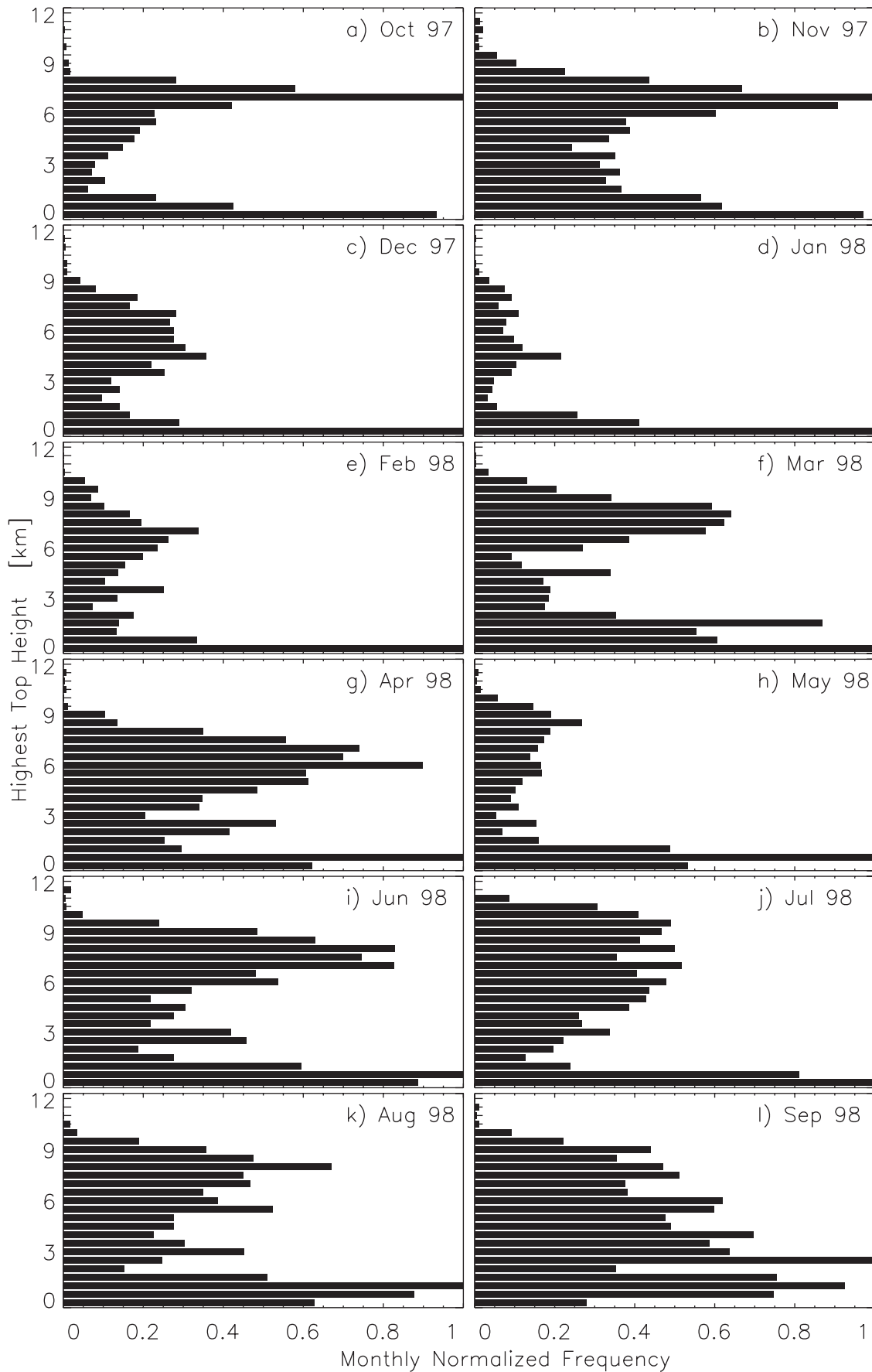
Figure 8. (a–l) Same as in Figure 6 but for highest cloud top height.
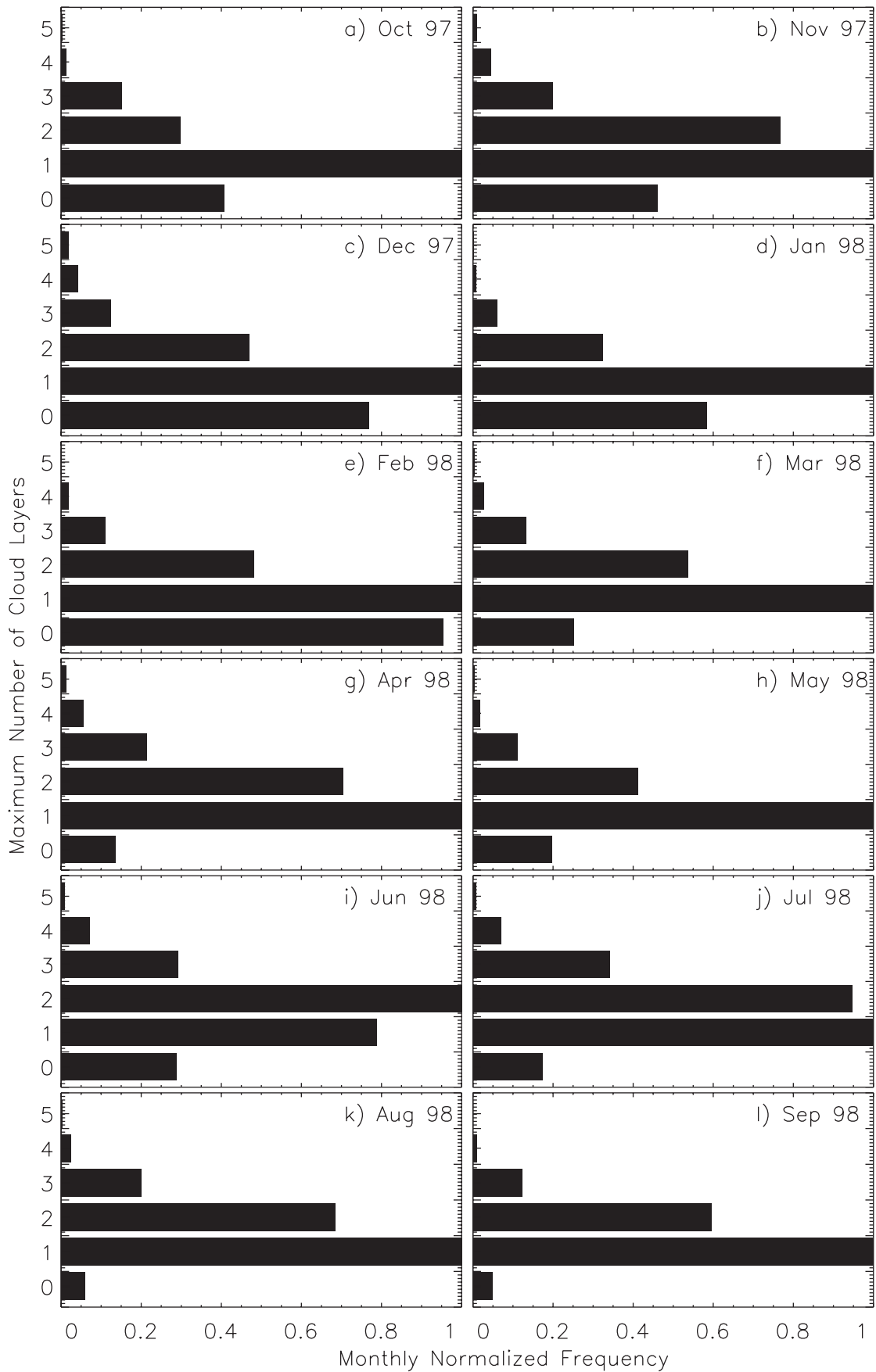
Figure 9. (a–l) Same as in Figure 6 but for maximum number of cloud layers. Bin size = 1. First bin = 0 layers corresponds to the percentage of time sky was clear.
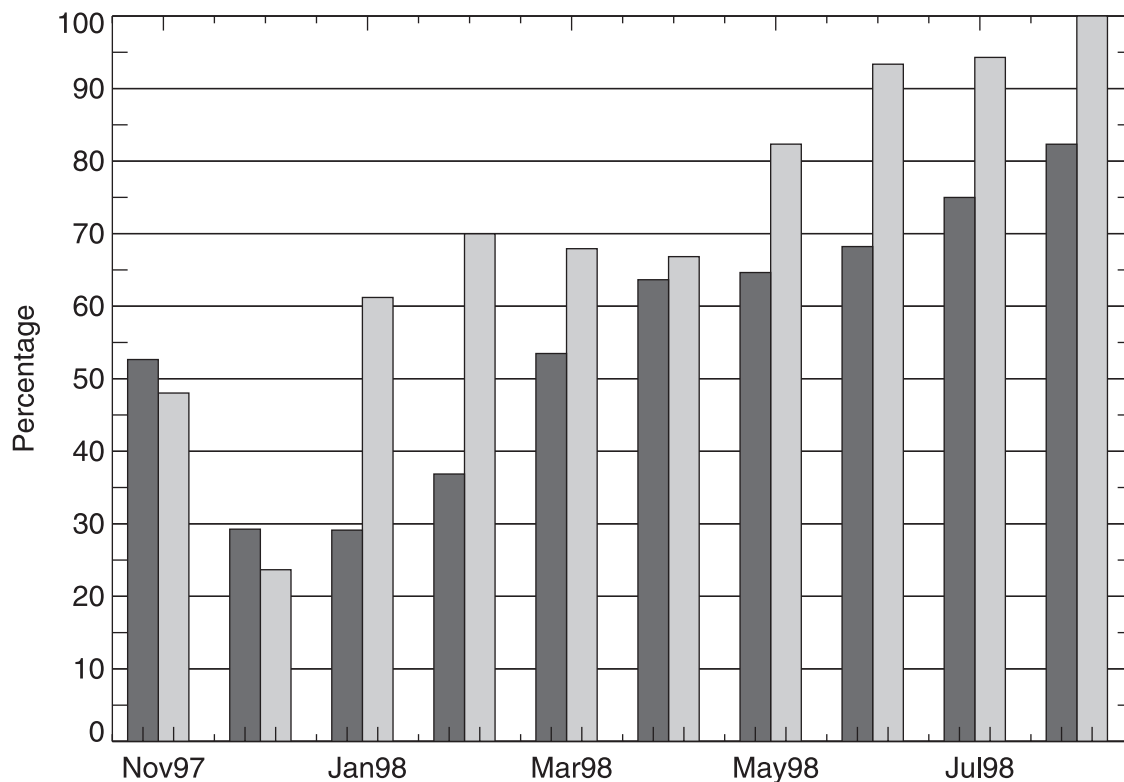
Figure 10. Monthly averaged percentages of clouds with liquid (light gray bars) and percentage of time that the lidar was attenuated (dark gray bars).

differences in location. Additionally, there are indicators that the SHEBA year was particularly stormy as a function of the year's El Nino event (J. A. Maslanik, personal communication) and therefore, perhaps cloudier.

4.2. Lowest Cloud Base and Highest Cloud Top Statistics

[24] Figure 6 shows the monthly averages of lowest cloud base and the highest cloud top obtained from the combined MMCR/DABUL data set. "Lowest cloud base" and "highest cloud top" are defined in the case of multiple layers as cloud base from the lowest layer and the cloud top from the highest layer, respectively. Therefore, for instance, if there were two layers, the cloud top from the lowest layer, and the cloud base from the upper layer are not included in the monthly statistics. This averaging procedure was chosen based on the reasoning that to a first order approximation, the lowest cloud base should be the most significant in effecting surface radiative fluxes, and the highest cloud top should be the first layer effecting top of the atmosphere fluxes.

[25] The lowest cloud base heights were variable throughout the year with monthly averages between 0.25 km agl (note: 0.25 km was the mean for both August and September and are most likely biased low since only radar bases were used) and 1.6 km agl with no distinct seasonal trend. Highest cloud top heights varied between 2.8 km and 5.5 km agl, with a slight tendency toward higher tops in the summer months and lower tops in the winter months.

[26] The monthly distributions of lowest cloud base heights as a function of altitude for October through September are shown in Figure 7. The highest frequency of occurrence of lowest cloud base was in the lowest 1 km of the atmosphere for all months indicating the prevalence of boundary layer clouds throughout the year. Most months showed a significant distribution of lowest cloud bases at higher levels in the atmosphere (November, December, February, March, April, and July). The months of January, May, June, August, and September, had significantly fewer incidences of the lowest cloud base occurring above the 1 km level.

[27] Figure 8 shows the corresponding monthly distributions of highest cloud top heights as a function of altitude for October through September. Highest cloud top heights were more evenly distributed throughout the atmosphere between 0 and 10 km agl than the lowest cloud base heights. All months, except September, showed bimodal distributions indicating the prevalence of both surface boundary layer clouds (tops between 0.5 and 1.0 km agl) and mid- and upper-level clouds (tops between 6 and 8 km agl).

4.3. Multiple Cloud Layers

[28] The Arctic is a region where several cloud layers can evolve and persist [*Herman and Goody*, 1976], especially in the spring and summer boundary layer. During SHEBA, stratus clouds were observed by the lidar to occur in up to five thin, but well defined, layers, however in general, the lidar and radar most often detected one or two cloud layers in the column. The number of cloud layers defaulted to the instrument which detected the greatest number of layers. Monthly histograms of the number of layers detected are
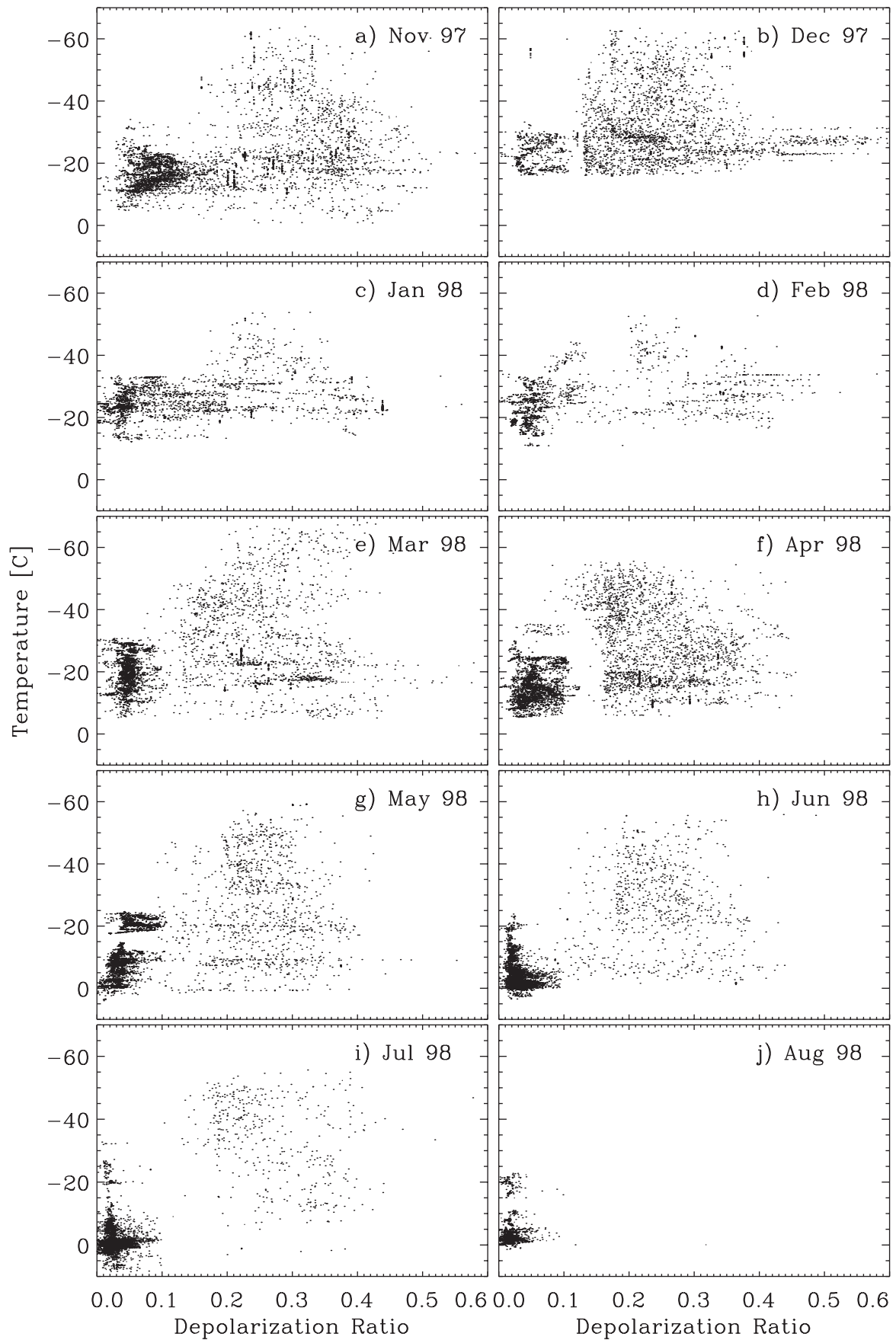
Figure 11.   (a–j) Lidar cloud depolarization ratio versus temperature (C) for each month.
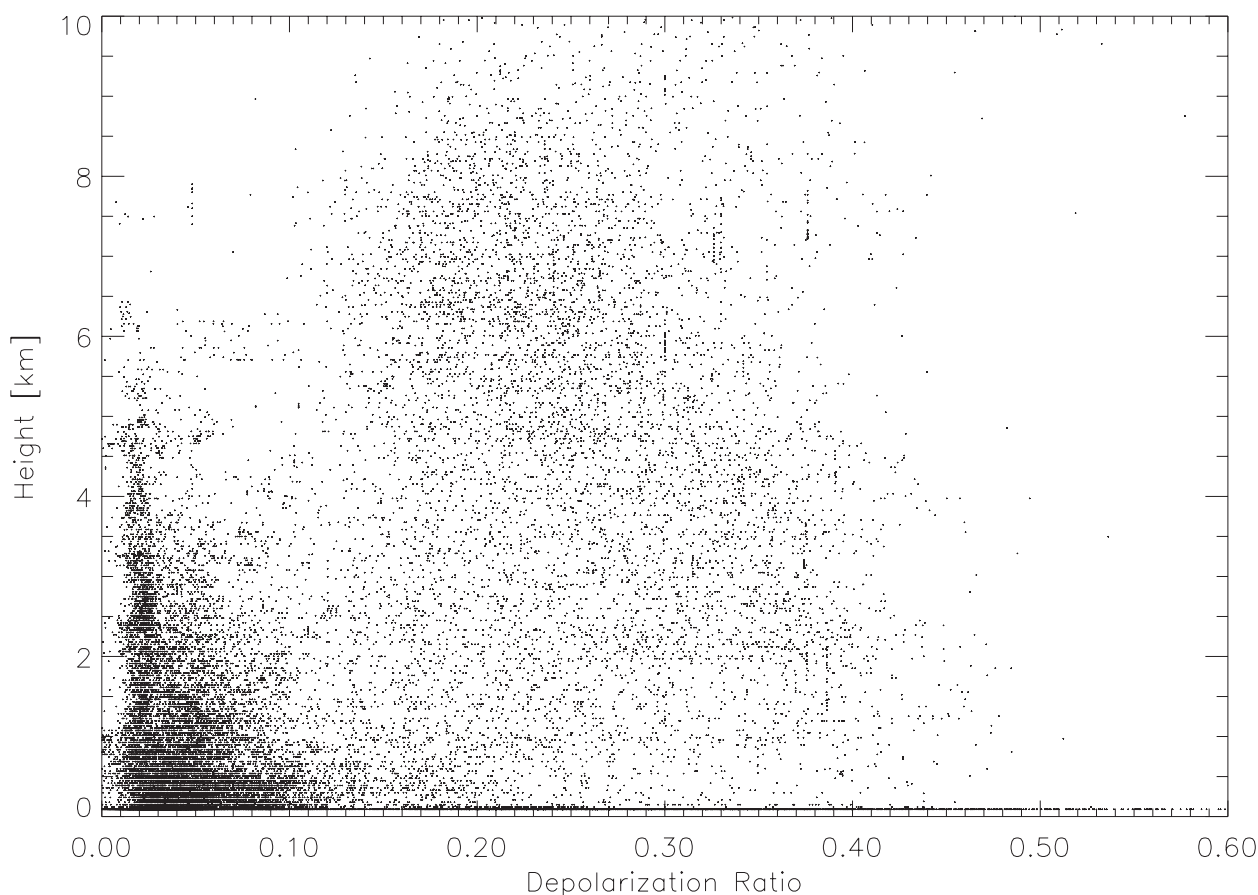
Figure 12. Scatterplot of lidar depolarization ratio versus height (km) from 1 November 1997 through 8 August 1998.

presented in Figure 9. Note that June and July were the only two months in which the fraction of time with multiple layers greatly exceeded the fraction of time with single cloud layers. June and July were also the months with the highest occurrence of four or more layers. In other months single layers were most prevalent, with the exception of November when the occurrence of multiple layers and single layers was approximately equal.

4.4. Liquid Water Statistics

[29] Correctly characterizing cloud phase is one of the most critical requirements for determining the radiative impact of clouds on the surface [*Sun and Shine*, 1994]. In general, the lidar detected liquid phase in clouds throughout the observational period (Figure 10). Although the occurrence of water in clouds was greater during the summer (95% for June through August), there was still a significant fraction of winter clouds with measurable amounts of liquid water (45% for November through February). During the spring (March through May) clouds contained liquid water 73% of the time that the lidar detected clouds. The smallest monthly fraction of clouds with liquid phase occurred in December (23%) and the largest occurred in July (95%). Note that liquid was detected 100% of the time in August, however this statistic is based on only 8 days of lidar observations. Liquid was observed in a variety of cloud types including thin water clouds precipitating ice crystals,

all-liquid water cloud layers, as well as true mixed-phase (ice crystals and water droplets coexisting in the same volume [*Hobbs et al.*, 2001]) clouds.

[30] Figure 10 also illustrates the amount of time the lidar signal was determined to be attenuated (based on the criteria that the highest radar echo was at least 200 m higher than the highest lidar return). In November and December, there were more attenuating events than liquid water events. This resulted from liquid-free snow storms where ice and snow precipitation was heavy enough to attenuate the lidar signal. In the remaining months of the year, liquid water events exceeded attenuating events. The difference between these two quantities indicates the amount of time during which the lidar was able to penetrate thin liquid layers; a condition that occurred most often in January and February. In general, as the occurrence of liquid water increased during the year the percentage of time the lidar was attenuated by the liquid also increased, indicating that liquid layers became optically thicker as they became more frequent.

[31] Figure 11 illustrates the monthly relationships between lidar depolarization ratio and cloud temperature, measured by radiosondes. Although there is significant scatter in these plots, general information on the relationships between temperatures and phase can be inferred. Using a cutoff 0.11 as a threshold between liquid and ice phase, as discussed in section 2, liquid tended to occur over wide temperature ranges which varied monthly (−13 to

−34°C in January; +10 to −30°C in July). Depolarization ratios indicating ice phase occurred over even larger temperature ranges which also varied seasonally (−15 to −60°C in December; 0 to −50°C in July).

[32] The relationship between depolarization ratio and cloud height is shown in Figure 12 for the full annual cycle. Depolarization ratios less than 0.11 (liquid) were generally concentrated within the lowest 1 km, were frequent up to 4.5 km agl, and were observed occasionally up to 6.5 km agl. Depolarization ratios greater than 0.11 (ice) were distributed evenly between the surface and 10 km agl.

5. Summary and Conclusions

[33] Arctic cloud occurrence, base and top echo boundary heights, number of layers and phase information were documented over an annual cycle by the NOAA/ETL cloud radar and depolarization lidar that were deployed as part of the SHEBA project. A cloud morphology data set was created using a combination of both the lidar and radar measurements, incorporating both instruments' detection strengths. These observations revealed that the Arctic atmospheric region sampled was cloudy about 85% of the year. The least amount of cloudiness occurred during the wintertime (∼70%) and the maximum cloud occurrence was observed during the summer (∼90%). Monthly averages of cloud base and top heights and number of cloud layers were also presented showing the echo base heights varied between 0.25 and 1.6 km agl and top heights ranged between 2.8 km and 5.5 km agl with little seasonal trend. The lidar and radar statistics indicated that the number of layers was typically between 1 or 2, with 2 or greater layers occurring more frequently in the spring and summer. Lidar measurements of depolarization ratios revealed that clouds with liquid water phase and mixed phase clouds existed throughout the SHEBA year, and through a wide range of temperature and altitude ranges, although it tended to be concentrated in the lowest 1 km of the atmosphere in the spring and summer months.

[34] The importance and necessity of using both lidar and radar measurements was demonstrated by documenting the unique contributions each instrument made to the combined cloud geometry data set. Radar-determined cloud top heights and lidar-determined cloud base heights were most often used in the combined product while both measurements contributed similarly to the determination of number of layers.

[35] Ongoing work incorporating the cloud morphology and phase information presented here are being pursued as part of many other studies: validation of satellite retrieval algorithms [*Key and Intrieri*, 2000; *Minnis et al.*, 2001; *Schweiger et al.*, 2001], comparisons with aircraft data [*Hobbs et al.*, 2001; *Khvorostyanov et al.*, 2001], model studies [*Beesley et al.*, 2000; *Bretherton et al.*, 2000] and surface cloud radiative forcing [*Intrieri et al.*, 2002]. Another application of this study is the use of the relative lidar-radar monthly cloud detection statistics to provide information for the satellite based program CloudSAT/CALIPSO [*Winker and Wielicki*, 1999] which plans to deploy a cloud lidar and radar, at the same wavelengths as those used in this study, into space.

References

Alvarez, R. J., III, W. L. Eberhard, J. M. Intrieri, S. P. Sandberg, and K. W. Koenig, Cloud backscatter and phase measurements in the Arctic using ETL's DABUL lidar, in *Proceedings 4th International Symposium on Tropospheric Profiling*, pp. 7–9, Am. Meteorol. Soc., Boston, Mass., 1998.

Beesley, J. A., C. S. Bretherton, C. Jakob, E. L. Andreas, J. M. Intrieri, and T. Uttal, A comparison of cloud and boundary layer variables in the ECMWF forecast model with observations at SHEBA, *J. Geophys. Res.*, accepted, 2000.

Bretherton, C. S., S. R. de Roode, C. Jakob, E. A. Andreas, and R. M. Moritz, A comparison of the ECMWF forecast model with observations over the annual cycle at SHEBA, *J. Geophys. Res.*, accepted, 2000.

Clothiaux, E. E., B. E. Martner, T. P. Ackerman, K. P. Moran, and M. A. Miller, Cloud detection by radar and lidar at the ARM CART sites, in *Proceedings Radar Conference*, Am. Meteorol. Soc., Boston, Mass., 2000.

Curry, J. A., and E. E. Ebert, Annual cycle of radiative fluxes over the Arctic Ocean: Sensitivity to cloud optical properties, *J. Clim.*, 5, 1267–1280, 1992.

Curry, J. A., W. B. Rossow, D. Randall, and J. L. Schramm, Overview of Arctic cloud and radiation characteristics, *J. Clim.*, 9, 1731–1764, 1996a.

Curry, J. A., J. O. Pinto, T. Benner, and M. Tschudi, Evolution of the cloudy boundary layer during the autumnal freezing of the Beaufort Sea, *J. Geophys. Res.*, 102, 13,851–13,860, 1996b.

Francis, J., Cloud radiative forcing over Arctic surfaces, in *Proceedings 5th Conference on Polar Meteorology and Oceanography*, pp. 221–226, Am. Meteorol. Soc., Boston, Mass., 1999.

Grund, C. J., and S. P. Sandberg, Depolarization and backscatter lidar for unattended operation, in *Proceedings 18th International Laser Radar Conference*, pp. 3–7, Springer, New York, 1996.

Hahn, C. J., S. G. Warren, and J. London, The effect of moonlight on observation of cloud cover at night and application to cloud climatology, *J. Clim.*, 8, 1429–1446, 1995.

Herman, G. F., and R. Goody, Formation and persistence of summertime Arctic stratus clouds, *J. Atmos. Sci.*, 33, 1537–1553, 1976.

Hobbs, P. V., and A. L. Rangno, Microstructures of low and middle-level clouds over the Beaufort Sea, *Q. J. R. Meteorol. Soc.*, 124, 2035–2071, 1998.

Hobbs, P. V., A. L. Rangno, T. Uttal, and M. Shupe, Airborne studies of cloud structures over the Arctic Ocean and comparisons with retrievals from ship-based 35 GHz radar and radiometer measurements, *J. Geophys. Res.*, 106, 15,029–15,215, 2001.

Intrieri, J. M., C. F. Fairall, M. D. Shupe, O. G. P. Persson, E. L. Andreas, P. L. Guest, and R. M. Moritz, An annual cycle of Arctic surface cloud forcing at SHEBA, *J. Geophys. Res.*, 107, 10.1029/2000JC000439, in press, 2002.

Key, J., and R. G. Barry, Cloud cover analysis with Arctic advanced very high resolution radiometer: cloud detection, *J. Geophys. Res.*, 94, 8521–8535, 1990.

Key, J., and J. M. Intrieri, Cloud particle phase determination with the AVHRR, *J. Appl. Meteorol.*, 39, 1797–1804, 2000.

Key, J., D. Slayback, C. Xu, and A. Schweiger, New climatologies of polar clouds and radiation based on the ISCCP D products, in *Proceedings 5th Conference on Polar Meteorology and Oceanography*, pp. 227–232, Am. Meteorol. Soc., Boston, Mass., 1999.

Khvorostyanov, V. I., J. A. Curry, and J. O. Pinto, Evaluation of an explicit microwave scheme using observations of an upper-level cloud system observed during FIRE.ACE, *J. Geophys. Res.*, 106, 15,099–15,112, 2001.

Maykut, G. A., and N. Untersteiner, Some results from time-dependant thermodynamic model of sea-ice, *J. Geophys. Res.*, 76, 1550–1575, 1971.

Minnis, P., D. R. Doelling, V. Chakrapani, D. A. Spangenberg, L. Nguyen, R. Palikonda, T. Uttal, R. F. Arduini, and M. Shupe, Cloud coverage and height during FIRE ACE derived from AVHRR data, *J. Geophys. Res.*, 106, 15,215–15,222, 2001.

Moran, K. P., B. E. Martner, M. J. Post, R. A. Kropfli, D. C. Welsh, and K. B. Widener, An unattended cloud-profiling radar for use in climate research, *Bull. Am. Meteorol. Soc.*, *79*, 443–455, 1998.

Perovich, D. K., et al., The Surface Heat Budget of the Arctic Ocean, *EOS Newslett.*, 1999.

Randall, D. A., Status of and outlook for large-scale modeling of atmosphere-ice-ocean interactions in the arctic, *Bull. Am. Meteorol. Soc.*, *79*, 197–219, 1998.

Sassen, K., The polarization lidar technique for cloud research: A review and current assessment, *Bull. Am. Meteorol. Soc.*, *72*, 1848–1866, 1991.

Schweiger, A., J. Francis, J. Key, J. Intrieri, and M. Shupe, Validation of TOVS Path-P data during SHEBA, *J. Geophys. Res.*, accepted, 2001.

Stokes, G. M., and S. E. Schwartz, The Atmospheric Radiation Measurement (ARM) Program: Programmatic background and design of the Cloud and Radiation Test Bed, *Bull. Am. Meteorol. Soc.*, *75*, 1201–1221, 1994.

Sun, Z., and K. P. Shine, Studies of the radiative properties of ice and mixed-phase clouds, *Q. J. R. Meteorol. Soc.*, *120*, 111–137, 1994.

Uttal, T., et al., The Surface Heat Budget of the Arctic Ocean (SHEBA), *Bull. Am. Meteorol.*, 255–275, 2002.

Vowinkel, E., and S. Orvig, The climate of the north polar basin, in *Climates of the Polar Regions*, vol. 14, *World Survey of Climatology*, edited by S. Orvig, 129–152, Elsevier, New York, 1970.

Warren, S. G., C. J. Hahn, J. London, R. M. Chervin, and R. L. Jenne, Global distribution of total cloud cover and cloud type amounts over the ocean, *Tech. Note NCAR/TN-317+STR*, 212 pp., Natl. Cent. for Atmos. Res., Boulder, Colo., 1988.

Washington, W. M., and G. A. Meehl, Climate sensitivity due to increased CO_2: Experiments with a coupled atmosphere and ocean general circulation model, *Clim. Dyn.*, *4*, 1–38, 1989.

Winker, D. M., and B. A. Wielicki, 1999: The PICASSO-CENA Mission, in *Sensors, Systems, and Next Generation Satellites*, edited by H. Fujisada, *Proc. SPIE*, 3870, 2636 pp., 1999.

_____

J. M. Intrieri and T. Uttal, NOAA/Environmental Technology Laboratory, Boulder, CO 80305, USA. (janet.intrieri@noaa.gov)

M. D. Shupe, Science and Technology Corporation, NOAA/Environmental Technology Laboratory, Boulder, CO 80305, USA.

B. J. McCarty, Cooperative Institute for Research in the Environmental Sciences, University of Colorado, Boulder, CO 80309, USA.
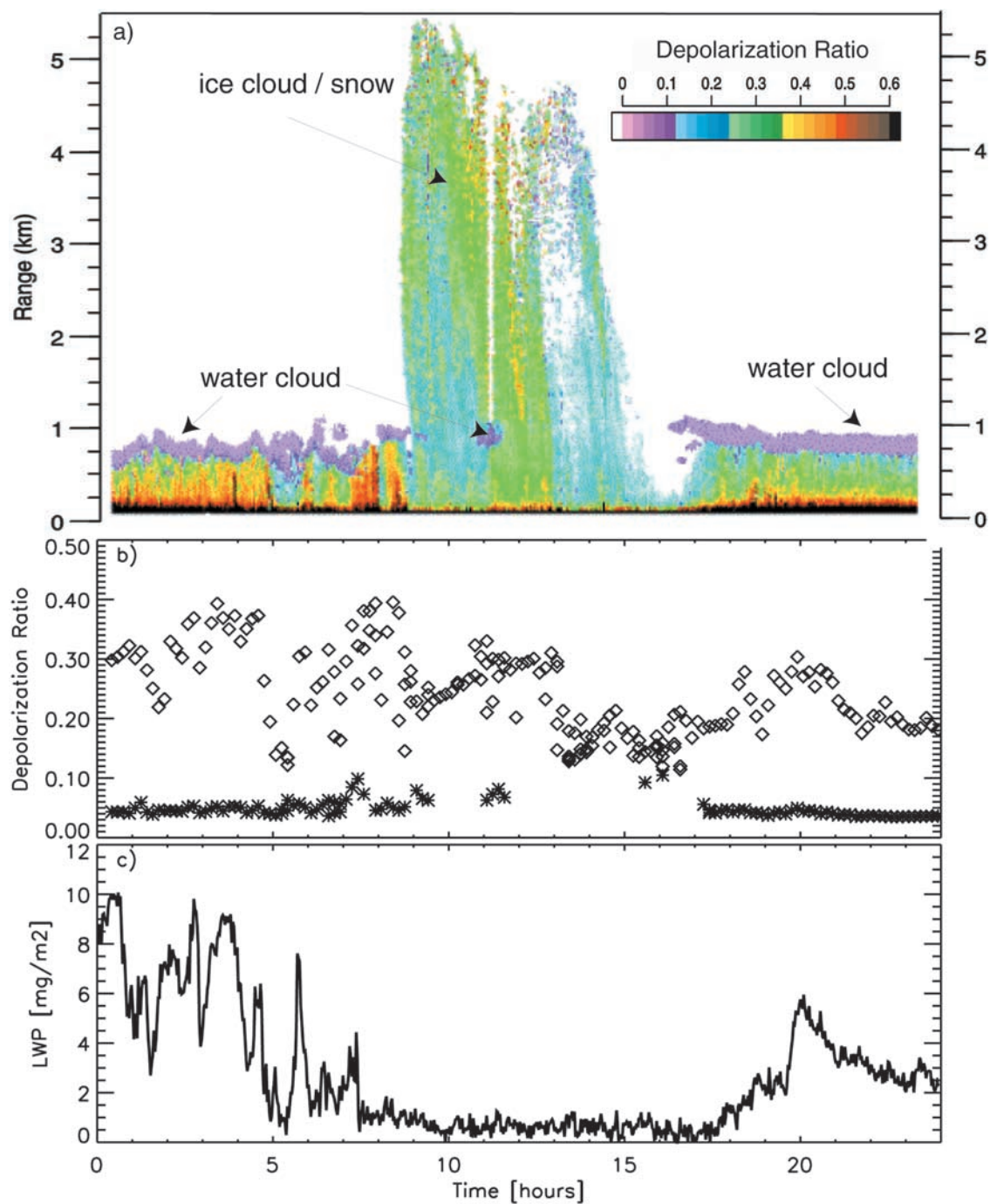
Figure 1. (a) Time-height plot of the lidar depolarization ratio field, (b) corresponding time series of the layer-average depolarization ratio values for the low level water cloud (asterisks) and ice crystal precipitation (diamonds), and (c) time series of microwave radiometer column liquid water amount (mg/m^2) for 6 May 1998.
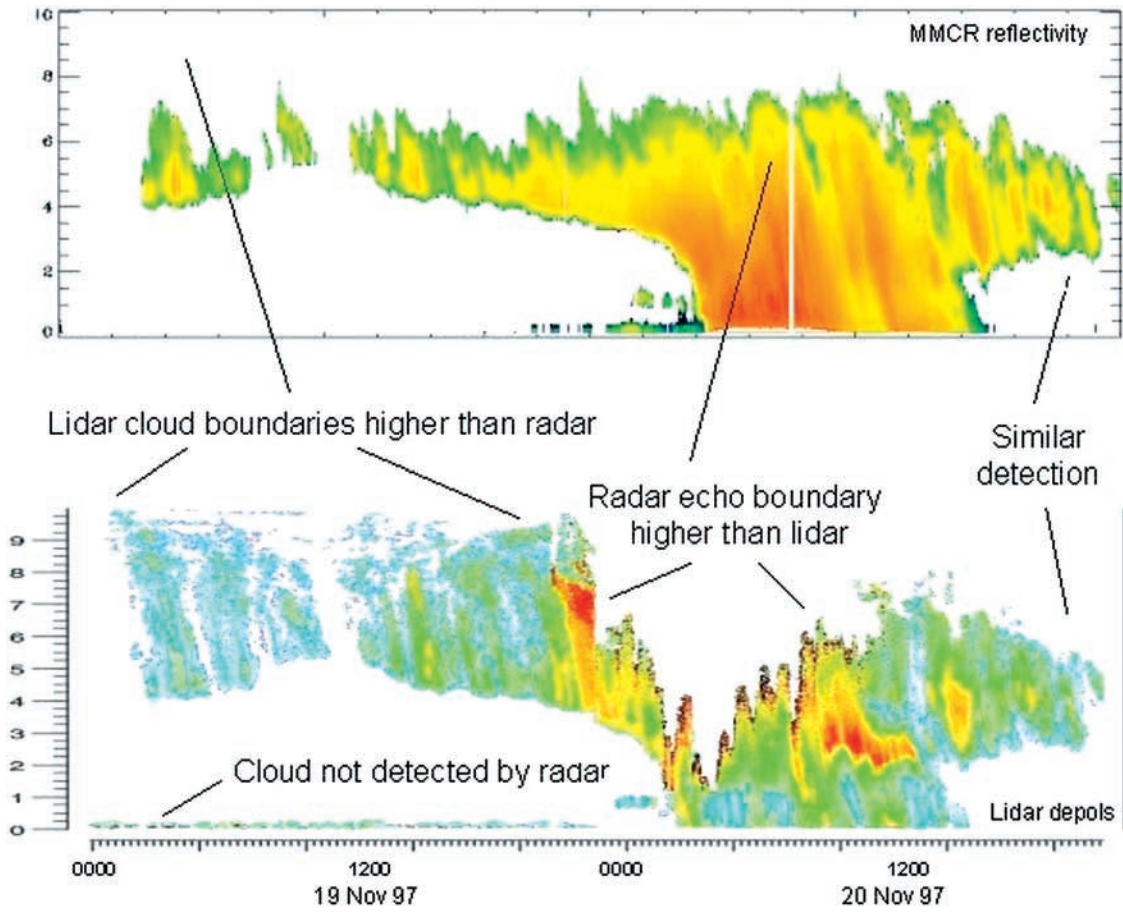
Figure 2. Two day time-height plot of radar reflectivity (top) and lidar depolarization ratio (bottom) for 19–20 November 1997 illustrating the similarities and differences in radar and lidar returns a variety of cloud types.